ISSN 2072-5981

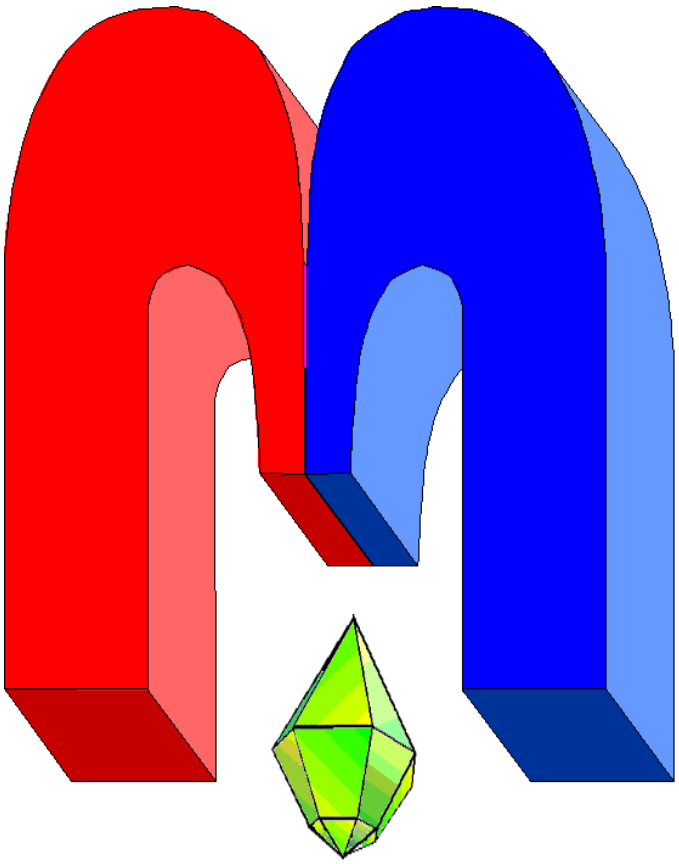

Magnetic Resonance in Solids

Electronic Journal

Volume ***19,***
Issue ***2***
Paper No ***17207,***
1-10 pages
2017

http://mrsej.kpfu.ru
http://mrsej.ksu.ru

Established and published by Kazan University
Sponsored by International Society of Magnetic Resonance (ISMAR)
Registered by Russian Federation Committee on Press, August 2, 1996
First Issue was appeared at July 25, 1997

"***Magnetic Resonance in Solids. Electronic Journal***" (**MRS*ej***) is a peer-reviewed, all electronic journal, publishing articles which meet the highest standards of scientific quality in the field of basic research of a magnetic resonance in solids and related phenomena.

Indexed and abstracted by
Web of Science (*ESCI*, Clarivate Analytics, from 2015), *Scopus* (Elsevier, from 2012), *RusIndexSC* (*eLibrary*, from 2006), *Google Scholar*, *DOAJ*, *ROAD*, *CyberLeninka* (from 2006), *SCImago Journal & Country Rank*, etc.

* In Kazan University the Electron Paramagnetic Resonance (EPR) was discovered by Zavoisky E.K. in 1944.

Conventional electron paramagnetic resonance for studying synthetic calcium phosphates with metal impurities (Mn^{2+}, Cu^{2+}, Fe^{3+})

F. Murzakhanov[1], B. Gabbasov[1], K. Iskhakova[1], A. Voloshin[1], G. Mamin[1], V. Putlyaev[2], E. Klimashina[2], I. Fadeeva[3], A. Fomin[3], S. Barinov[3], T. Biktagirov[1,4], S. Orlinskii[1], M. Gafurov[1,*]

[1] Kazan Federal University, Kremlevskaya 18, Kazan 420008, Russia

[2] Lomonosov Moscow State University, GSP-1, Leninskie Gory, Moscow, Russia

[3] Baikov Institute of Metallurgy and Materials Science, Leninskii Pr. 49, Moscow, Russia

[4] University Padeborn, Warburger Str. 100, Padeborn, Germany

**E-mail: Marat.Gafurov@kpfu.ru*

(Received November 23, 2017 ; revised December 17, 2017;
accepted December 19, 2017; published December 27, 2017)

Calcium phosphate (CaP) based materials are widely recognized as the most suitable matrix for bone tissue engineering. The cationic and anionic substitution of CaP structure by the elements and groups of biological importance is the effective way to improve the properties of CaP based substances to achieve the material's desired parameters. Some aspects of application of the conventional electron paramagnetic resonance (EPR) approaches for characterization of CaP powders and ceramics such as hydroxyapatite (HAp) and tricalcium phosphates (TCP) containing intrinsic impurities or intentional dopants like manganese, copper, iron are demonstrated. It is shown that the radiation induced EPR spectra for the nominally pure HAp and TCP reveal the presence of stable nitrogen containing or hydrogen radicals and depend on the CaP synthesis route. It is found that the experimental values of the hyperfine splitting (A) for the nitrogen containing radicals in TCP differ from those known for HAp. The observed narrowing of the central EPR line and increase of its amplitude with the concentration of Mn^{2+} in the range from 0.05 up to 5 wt. % could be exploited for the quantitative determination of manganese in CaP. Analysis of the EPR spectra of the iron containing CaP allows to determine the presence of iron in Fe^{3+} state. The values of the components of g and A for Cu^{2+} ions in TCP are determined and it is demonstrated that they can be influenced by the presence of the codoped Mn^{2+}. Therefore, conventional EPR can be used to study cation-cation codoping.

PACS: 83.80.Lz, 87.64.-t

Keywords: hydroxyapatite, calcium phosphates, tricalciumphosphate, ENDOR, EPR

1. Introduction

Calcium phosphates (CaP) are interesting compounds in many fields of science, including geology, chemistry, biology and medicine due to its abundance in the nature and presence in the living organisms [1-6]. CaP materials with different functional features such as biocompatibility, catalytic activity, ion conductivity may be formed by a cation or/and an anion substitution within initial matrix. Pigmentation is one more characteristic established recently for the CaP modified by lanthanide [7, 8] which makes this substance promising to be used for the development of bioactive materials for bone regeneration and smart fluorescent probes for bio imaging applications.

During the bone growth and formation, calcium ions can be partially replaced by ions of trace elements. Copper is an essential redox metal ion figuring as a cofactor for intracellular enzymes involved in a number of physiological processes, ranging from signal transduction to energy generation and from oxygen transport and cell metabolism to blood clotting [9]. Its deficiency or disrupted homeostasis are directly linked with disease states [10]. As far as its effect on bone health is concerned, copper shortage decreases bone strength [11], while its use as a diet supplement reduces bone loss in menopause [12, 13]. Alongside having a role in mineralization, copper is a cofactor for lysyl oxidase, an enzyme crosslinking collagen fibers and increasing the integrity of the bone connective tissue [14].

Manganese is an essential trace element to human health. Mn deficiency leads to lower thickness and length of newly formed bones. The presence of manganese in HAp structure is able to change the adherence of bone cells to an implant material and favors osteoblasts activity and proliferation [15].

The study of Sopyan et al. [16] revealed that increasing Mn content lowers the crystallization temperatures of hydroxyapatite (HAp, $Ca_{10}(PO_4)_6(OH)_2$) and accelerates tricalcium phosphate (TCP, $Ca_3(PO_4)_2$) formation through the decomposition of HAp. It is speculated that the concentration of paramagnetic Mn^{2+} in the inorganic component of the aorta atherosclerotic plaques (composed mainly of the carbonated, non-stoichiometric hydroxyapatite) depends on the plaque stability and, therefore, can serve as a surgical indication [17]. Besides the biologically relevant applications of Mn-doped CaP, the experimental results indicate that HAp/MnO_2 composite may be an effective adsorbent for the removal of lead ions from aqueous solutions [18], while the HAp supported Mn can serve as precursor for the oxide catalysts [19]. Mn^{2+} has an ionic radius close to the Mg^{2+} and could serve as a magnetic analog in order to study Mg^{2+} doped CaP materials by magnetic resonance methods, including electron paramagnetic resonance (EPR). Incorporation of Mn^{2+} as well as Cu^{2+} ions is a promising way to obtain biomedical bone and dental materials with antibacterial properties [20].

The high concentrations of iron is present in soft organs of human body whereas in hard tissues it is present in very low concentration without disturbing the apatite structure. Function of iron ions incorporated in bone and teeth enamel is not well studied; incorporation of iron into HAp has not been thoroughly investigated and still remains an area of research to be developed. The biomagnetic nanoparticles of CaP with the incorporation of iron ions exhibit strong ferromagnetic or suprapara-magnetic properties. Fe-HAp systems play an important role in medicine and could be useful for biological applications such as magnetic resonance imaging (MRI), cell separation, drug delivery and heat mediator for the hyperthermia treatment of cancer [6, 21]. Toxicity of iron oxides from using Fe-HAp is a significant concern and also under the serious consideration.

Since recently simultaneous codoping of CaP by various ions and groups to achieve the desired antimicrobial, mechanical, chemical properties to fulfill the requirements of the personalized medicine attracts great attention [22-24]. Evidently, the presence of the other dopants may lead to the inhomo-geneous distribution of the target ions and groups, affects their release and uptake. Therefore, the morphology and functionality of the co-doped CaP could differ significantly from the individually doped. For example, the authors of [25] showed that the standard purification procedure by thermal annealing of HAp based catalysts to remove undesirable nitrate ions is not operational as soon as Mn^{2+} ions are used to enrich the surface active sites. Furthermore, the incorporation of part of NO_3^- in the hydroxyapatite promoted the surface Ca^{2+} enrichment by the incorporation of Mn^{2+} into the HAp support. The results are in agreement with the experimental and theoretical conclusions of our paper [26] based on EPR measurements. In our previous papers [26-28] we presented the "mutual" influence for the anion-anion ($CO_3^{2-} - NO_3^-$) and cation-anion ($Mn^{2+} - NO_3^-$) codoping of HAp by EPR experiments and density functional theory (DFT) calculations.

Despite the large number of the performed studies, many important problems relating to anionic and cationic substitutions even in HAp are not sufficiently investigated. Moreover, the data of different studies are incompatible. The more contradictory information is associated with the sites of the ions localization in biomineral, synthetic and nanosized samples. Due to the complex structure of tricalcium phosphate and plenty of possible sites for the ionic incorporation even comparing to the hydroxyapatite, substitutions in TCP are practically not investigated.

Another aspect of interest is an investigation of the normal and pathological calcified tissues. Because of CaP being an absorptive material, it is believed that this biomineral would actively absorb metal complexes that are present in the tissue matrix as the result of release from normal or destructive cells. Among those are the complexes of Fe, Cu, and Mn many of which are paramagnetic. The observed paramagnetic complexes may serve as intrinsic probes that show the origin, growth and status of the calcified biominerals as well as a status of the adjacent tissues. It is worth noting that quantitative determination of manganese in calcified materials is still a challenge for the analytical tools because of the structural and chemical complexity of the investigated matrices.

In this work we examine nominal pure synthetic HAp and TCP as well as doped by Fe, Cu, and Mn with conventional EPR in order to demonstrate some additional (or not well-known) abilities of the established technique to characterize CaP systems.

2. Materials and Methods

Mn^{2+} containing HAp samples (MnHAp powders) with the chemical formula $Ca_{10-x}Mn_x(PO_4)_6(OH)$ (Mn-HAp) were synthesized by the wet precipitation technique. Calcium nitrate monohydrate $Ca(NO_3)_2•H_2O$ (235 g) was dissolved in 420 mL of 20 % NH_4OH (solution A) while $(NH_4)_2HPO_4$ (72.2 g) was dissolved in 380 mL of deionized water (solution B). After the $(NH_4)_2HPO_4$ was completely dissolved, 30 mL of 20 % NH_4OH was added. Mn-containing reagent ($MnSO_4•H_2O$) was dissolved in 100 mL of deionized water and then added to the solution A. Then solution B was added to the manganese containing solution A and had been mixed by a magnetic stirrer for 24 h. After the mixing the precipitate was allowed to age for 48 h. Subsequently, the supernatant was decanted and then washed with 2.5 L of deionized water three times to remove the excess of NH_4OH and NO_3^-. The washing procedure was repeated three times. After the washing the MnHAp precipitate was separated from the liquid by filtering through a Buhner funnel. A part of the MnHAp precipitate had been heated at 900 °C for 3 h to remove residual NH_4NO_3 and improve crystallinity. In this work we investigate four samples with the nominal concentrations of 0.05; 0.1; 1 and 5 wt. %.

Pure TCP in its β form and its substituted powders were obtained using a precipitation technique according to the following reaction scheme:

$$(3-x)Ca(NO_3)_2 + x\,M(NO_3)_2 + 2(NH_4)_2HPO_4 \rightarrow Ca_{3-x}M_x(PO_4)_2, \quad (1)$$

where M = Cu^{2+}, Fe^{3+}, Mn^{2+} and x is varied in the range from 0 to 0.1.

The samples were characterized by infrared spectroscopy (IR, Nikolet Avatar 330), atomic emission spectroscopy (AES) and mass spectroscopy (MS) with inductively coupled plasma (ICP, Bruker Ultima 2 and Perkin Elmer ELAN DRC II) and the X-ray difractometry (Shimadzu 6000, Bruker D8 Advance, Rigaku D/Max-2500). A limited amount of “pure” TCP were synthesized by the solid state reaction technique. More details for the sample preparation, their post-synthesis treatment and analytical characterization are given in papers [26, 29].

X-ray irradiation of the synthesized powders was provided by using URS-55 tube (U = 55kV, I = 16 mA, W anticathode) at room temperature with the estimated dose of 10 kGy to create stable paramagnetic centers in the nominal pure TCP and HAp to have an ability to apply different EPR techniques. EPR measurements were done by using X-band (the microwave frequency ν_{MW} of 9.2-9.7 GHz) Bruker Elexsys 580 and table-top LABRADOR (Ekaterinburg, Russia).

3. Results and Discussion

3.1 Conventional EPR of the nominal pure TCP and HAp

Pure TCP and HAp are supposed to be EPR silent. Consequently, EPR can be used for the purity check and quantitative analysis of the doped CaP materials. A number of our papers are devoted to the investigation of HAp synthesized by the wet precipitation techniques from the NO_3 containing salts and acids [26, 28, 30, 31]. We, according to the previous published papers, have shown that EPR can detect the presence of nitrate impurities while the established IR techniques sometimes are not (the nitrate bands in the vicinities of 825 and 1385 cm^{-1} are not revealed).

In the irradiated HAp samples EPR is mainly due to the stable NO_3^{2-} ions preferably substituting one of the PO_4^{3-} position in the HAp structure (substitution of B-type). Their powder EPR spectra can described by the spin-Hamiltonian of the axial symmetry:

$$H = g_{||}\beta B_z S_z + g_{\perp}\beta(B_x S_x + B_y S_y) + A_{||} S_z I_z + A_{\perp}(S_x I_x + S_y I_y), \quad (2)$$

where $g_{||}$ and $g_{\perp}$ are the main components of the g tensor, $A_{||}$ and $A_{\perp}$ are the main components of the

hyperfine tensor, B_i, S_i and I_i are the projections of the external magnetic field strength, $S = 1/2$ and $I = 1$ are electronic and nuclear spin correspondingly onto the $i = \{x, y, z\}$ coordinate axis, β is a Bohr magneton. The HAp spectra could be simulated properly if we suppose a Gaussian (continuous) distribution of $A_{||}$ with a deviation of 0.40 mT around the mean value of 6.65(40) mT and a discrete distribution of $A_{\perp}$ (three partially resolved lines) from 3.2 to 3.6 mT, while the components of g-factors for all of the obtained radical's modifications are the same ($g_{||} = 2.0011(1)$, $g_{\perp} = 2.0052(1)$) [30].

Fig. 1a demonstrates that EPR spectrum of the wet synthesized TCP after radiation is also mainly due to the NO_3^{2-} radicals and could be described by the same g-factors as for the HAp. But the values of the observed hyperfine splitting differ. Supposing, as usual, that A_1 is 2 times $A_{||}$, $A_{||} = 6.15(10)$ mT which is less than that for the HAp (see previous paragraph) and is closer to the value for the "free" nitrate radical (5.75 mT [30]). Three resolved lines with $(A_2, A_3, A_4) = (4.8, 5.8, 6.7)$ mT is to obtain. Only the value of A_4 is close to that for the HAp while (A_2, A_3) are less. It could be due to the three different positions for PO_4 group substitution in TCP structure (Fig. 2) as well as due to the various schemes of the charge compensation. Presence of other nitrogen containing radicals such as NO_2, for

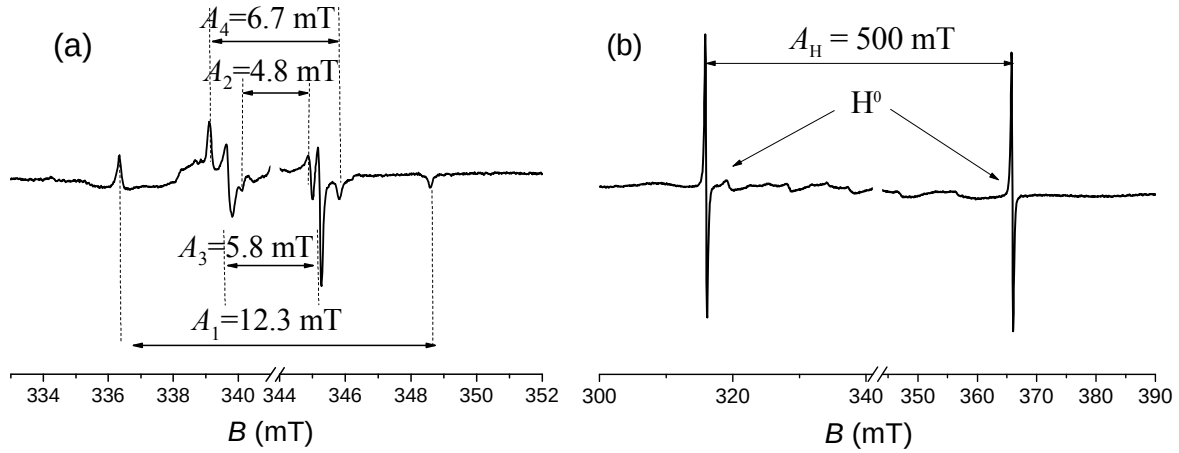

Figure 1. Conventional room temperature X-band EPR of the X-irradiated "pure" β-TCP synthesized by (a) the wet precipitation technique according to Eq. (1) and (b) solid state reaction technique. EPR lines in the central part of the spectra are cut for the clarity of the visual representation.

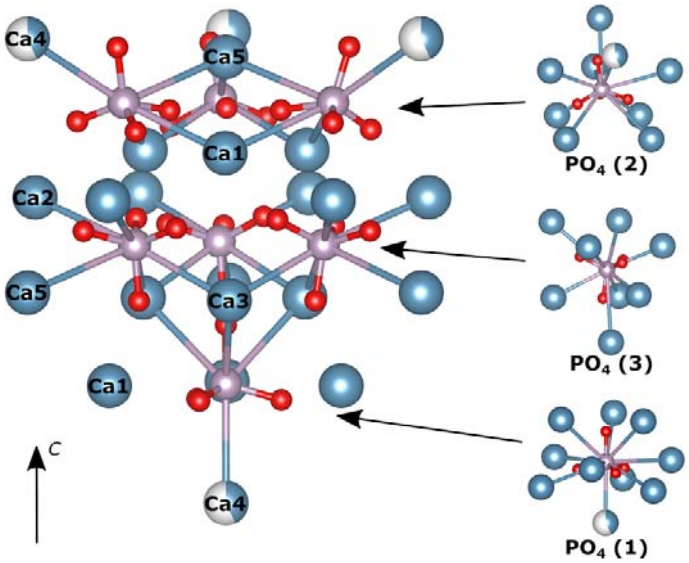

Figure 2. Representation of the TCP structure. Oxygen atoms are shown as small red balls, phosphorous as purple balls, calcium atoms as big blue balls. Five different calcium positions and three PO_4 positions are marked. Ca_4 position has a probability of occupation of about 50 % in TCP.

example, could not be excluded. Indeed, the literature review and own DFT calculations for HAp [30] show that $A_{||}$ for NO_2 and NO_2^{2-} differ in HAp from the corresponding fully "free" (isolated) radicals and is in the range of 3.9-6.6 mT. It is assumed that NO_2 and NO_2^{2-} are less stable than NO_3^{2-} and they are not observed in HAp, but for TCP the situation might be distinct. The corresponding calculations for TCP are on the way.

Solid state synthesized TCP as well as HAp after irradiation give rise to the intensive EPR lines with the splitting of about 500 mT due to the H^0 ($I = 1/2$) paramagnetic centers (Fig. 1b). This centres are less stable than the nitrogen ones and disappear (within the accuracy of our measurements and sensitivity limit of the spectrometer) after annealing at $T = 450$ K during 2 h. The remarkable differences for TCP and HAp produced by various methods could be exploited for the fairy simple identification of the content and synthesizing route of the commercial CaP materials, for example [32] which is often a proprietary information.

3.2. Conventional EPR of the doped TCP and HAp

One of the EPR features (in addition to the fact that it is a non-destructive method) is the high selective sensitivity to the mentioned paramagnetic complexes of Mn, Fe and Cu (Figs. 3, 4, 5). Consequently, EPR can be used for the quantitative analysis of the doped CaP materials.

Generally, the Mn^{2+} and Fe^{3+} CaP systems could be described by the spin-Hamiltonian

$$\hat{H} = g\beta\mathbf{BS} + D[S_z^2 - S(S+1)/3] + E(S_x^2 - S_y^2) + A\mathbf{SI}, \quad (3)$$

where $S_{x,y,z}$ are the projections of the electronic spin $S = 5/2$ on the principal direction of D; D and E are the commonly used (axial and orthorhombic, correspondingly) parameters for zero-field interaction (interaction with the crystal field); other parameters are defined above in the text. For simplicity we assume that the main axes of g, A and D tensors coincide. Function *pepper* of the EasySpin program was used to describe the powder spectra [33]. For Mn^{2+} it gives: $g = 2.01$, $D = 53(4)$ mT, $E = 14(3)$ mT. Because for ^{55}Mn the nuclear spin $I = 5/2$, six lines ($2I + 1 = 6$) of partially resolved hyperfine (HF) structure of Mn^{2+} with the isotropic HF constant with $A_{iso} \approx 9.0(4)$ mT are to obtain at top of the central one. It follows that $E / D \approx 0.27$, i.e. the system is quite anisotropic like glass [34]. Nevertheless, the g and A tensors could be taken isotropic and XRD analysis (within its accuracy) does not reveal any traces of the amorphous phases.

Very often the observation and interpretation of the HF structure (HFS) is rather complicated task. Even in the perfect crystals the resolution of the HFS spectra, the number of the components of the structure, their relative intensities strongly depend on the concentration of paramagnetic centers,

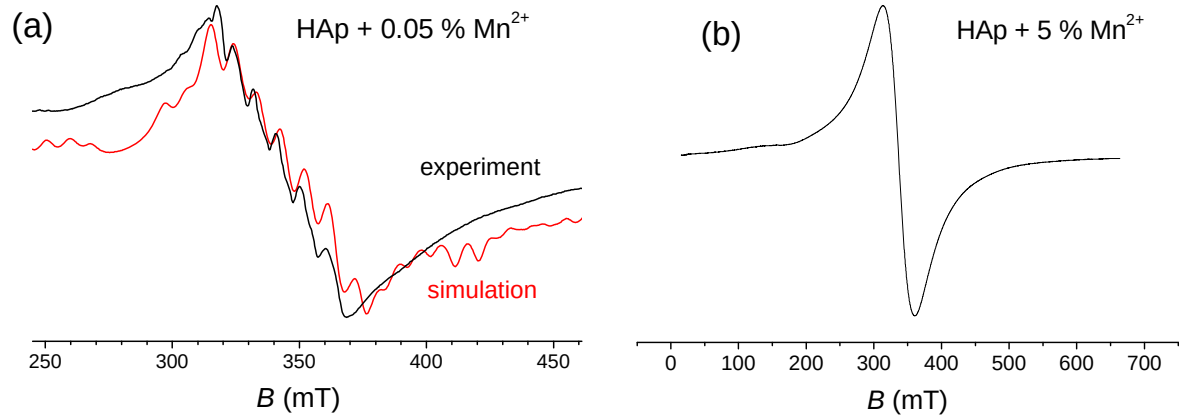

Figure 3. Comparison of EPR spectra for the manganese doped HAp at $T = 300$ K for (a) 0.05 %, only central part along with the corresponding simulation is shown; and (b) 5 %. Six lines of the partially resolved hyperfine structure due to $I = 5/2$ for ^{55}Mn nuclei is to observe for 0.05% Mn^{2+}. The signal amplitudes (vertical axes) are normalized for visibility. Parameters of the simulation curve are given in the text.

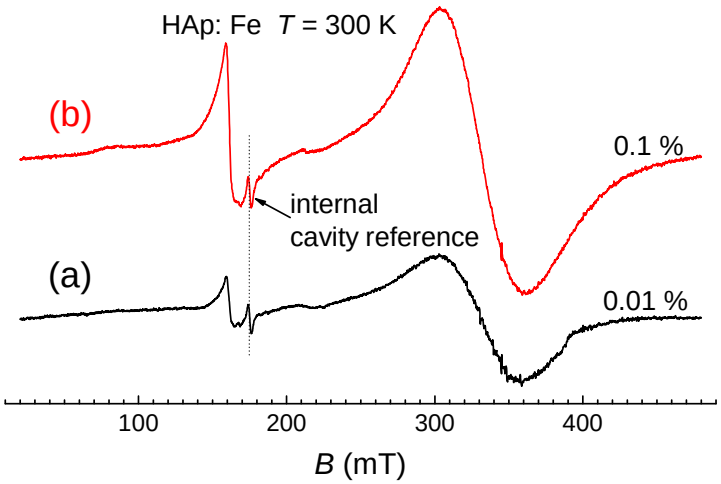

Figure 4. Comparison of EPR spectra for Fe doped HAp at $T = 300$ K for (a) 0.01% and (b) 0.1% concentrations. Signals at (100-160) mT indicate that iron is partially in Fe^{3+} state. Position of the impurity signal from the EPR cavity which served as a reference one is marked.

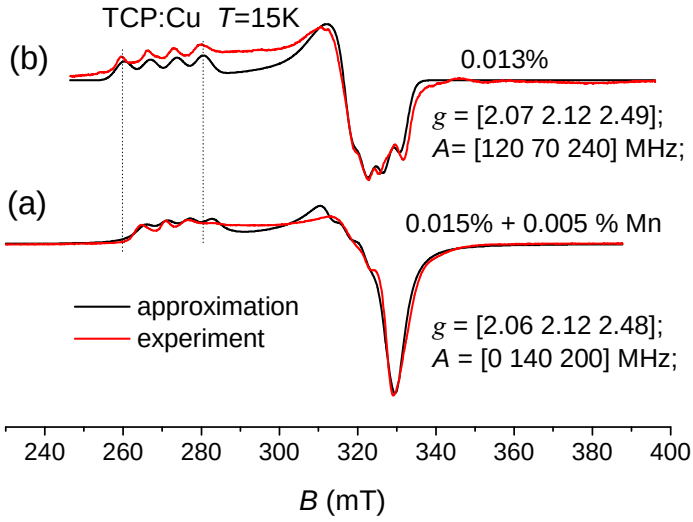

Figure 5. Comparison of EPR spectra of Cu doped β-TCP at $T = 15$ K. During the synthesis, one sample (a) was codoped with a small amount of manganese that slightly changed the EPR pattern, values of g components and hyperfine (A_z) splitting compared to the "pure" Cu doped TCP (b). The concentration of Cu^{2+} was derived after the double integration of EPR spectra compared to the reference one with the known concentration. The presence of manganese and Mn^{2+} ions in concentration of less than 0.005 % was proved by elemental analysis, ENDOR and W-band (94 GHz) measurements. Vertical dashed lines are drawn to show the difference visually.

orientation of the applied magnetic field and the EPR frequency [35-38]. That is why, for example, the resolved HFS of Mn^{2+} or HFS for Cu^{2+} ions in the (x, y) plane (corresponding to the perpendicular orientation of **B** to the main axes of g tensor) are rarely observed at X-band in the disordered systems (powders, ceramics, glasses, nanosized samples, inhomogeneous samples of biogenic origin, samples containing non-crystal amorphous phase, etc.) and a transition to the higher frequencies are necessary to interpret the EPR spectra correctly [35-37, 39]. Low manganese concentration allows us to obtain a resolved structure even in the X-band experiments (Fig. 3).

Though the increase of amount of paramagnetic complexes is followed by the raise of signal intensity, due to the electron spin-spin interaction the high concentrations of dopants could lead to the broadening of EPR lines and hinders the unambiguous interpretation of EPR spectra. For example, EPR pattern of TCP and HAp + 1 % Mn^{2+} resembles that for 0.01 % of iron (cf. Figures 3 and 4).

Table 1. Comparison of ICP MS data with the relative intensity of the central EPR line in HAp: Mn system after the double integration.

Nominal concentration, wt. %	M_{Mn}/M_{Ca} from ICP MS (relative values)	Relative integral intensity of the central EPR line
0.05	1	1
0.1	1.86(6)	1.8(1)
1	18.53(4)	19(1)
5	99.69(5)	96(3)

Concerning Mn^{2+} doped HAp and TCP, at high concentrations only central peak which mainly corresponds to the allowed transition with $\Delta M_s = -1/2 \leftrightarrow +1/2$ around $g \approx 2.0$ remains dominate.

Analysis of Mn^{2+} lineshape in HAp and TCP show that it is well fitted by the only Lorentzian curve for 5 % Mn^{2+} while at the lower concentrations a Gaussian contribution appears. The central peak in HAp narrows with concentration from 119 mT for 5 % down to 92 mT for 0.05 % for the halfwidth on the half peak, $\Delta H_{1/2}$ that could be used for the rough estimation of Mn^{2+} concentration or its change during the release, for example, adsorption processes in catalytic processes [40] (the results are not shown as a graph). The similar behavior is to obtain for TCP. The observed narrowing in papers [35, 36] was connected with the exchange interaction through the oxygen bridges. Exact analytical equation for describing the obtained dependence is still not developed.

We asked ourselves if it would be possible to use the intensity of only the central peak (after double integration) to calculate the concentration of Mn^{2+} from EPR. In general, it is not a case – one has to consider the full EPR spectrum taking into account all possible transitions with their probabilities. But the excellent concurrence of the EPR calculations with ICP MS data (Table 1) confirms that such simple way is applicable at least for the investigated concentration range. This is of particulary important for the specialists who use small (table top) types of EPR spectrometers like LABRADOR (Ekatirenburg, Russia) or Bruker escan: they are able to sweep the magnetic field only in the narrow field range (as a rule around $g \approx 2$). As we show even that is enough to estimate the concentration of Mn^{2+} in HAp from the intensity and linewidth of the central manganese peak.

Conventional room temperature X-band EPR could be used for the detection of iron in Fe^{3+} state in CaP as Fig. 5 presents. In this sense EPR complements the abilities of Mössbauer spectroscopy for the low iron concentrations and small amount of CaP samples [41].

Not only a role of iron in the biological apatites but even the structure of the iron paramagnetic complexes and their position in HAp or TCP structures are still a matter of controversy. From DFT calculations it follows that for HAp hexagonal Ca(2) position is preferable for Fe^{2+} substitution while Fe^{3+} should readily occupy Ca(1) position [42]. The reports from the experimental groups indicate that most probably iron introduces HAp as Fe–O–OH complex or within the impurity phases [43]. From that it could be not so easy to make a parallel with TCP – this material does not contain hydrogen or OH groups and has five calcium positions for substitution by "single" cations. Another feature of CaP: Fe systems is a supraparamagnetism, giving rise to huge magnetic signals in a wide range of the magnetic fields, especially in the vicinity of $g \approx 2$ (Fig. 4) even at low iron concentrations. Depending on synthesis route, post synthesis treatment, storage conditions, iron concentration, EPR detection conditions, etc. the intensity and lineshape of the signal at $g \approx 2$ changes drastically, that is a matter of the ongoing research along with the application of the multifrequency EPR experiments [44, 45] to unravel the structure of the iron paramagnetic complexes in HAp.

In case of even slight anisotropy of magnetic interaction tensors, EPR can provide the information about their orientation dependency and thereby about the spatial structure of the paramagnetic complexes in disordered systems. For copper both stable isotopes ^{63}Cu and ^{65}Cu have $I = 3/2$ and close

magnetic moments. This and the known anisotropies of the spectroscopic parameters g and A for Cu^{2+} in different matrices directly allow to assign presented in Fig. 5 spectra to Cu^{2+} due to 4 lines detected at $g_z \approx 2.4$ with $A_z \approx 200$-250 MHz. The Cu^{2+} spectra can be fitted well by using the spin-Hamiltonian of the rhombic symmetry like described by Eq.(2) for the axial one with the parameters of $g_z = 2.490$; $g_y = 2.118$; $g_x = 2.071$; $A_z = 240$ MHz; $A_y = 70$ MHz; $A_x = 120$ MHz.

Because the spectral and relaxation characteristics of paramagnetic complexes are very sensitive to the changes in the local environment it could be used for studying codoping effects even if the EPR spectrum of the second (or the third) codopant is not detected because of the low concentration or of an overlapping with the components of other paramagnetic centre(s). Figure 5 illustrates that the hyperfine splitting for Cu^{2+} in z direction (as the most resolved one) changes with Mn^{2+} addition though the Mn^{2+} spectrum is probably of low intensity and overlaps with the (x, y) components of Cu^{2+} one. It is usually assumed that divalent ions in TCP structure occupy Ca5 site in TCP structure (Fig. 2) while Ca4 is the second probable position for substitution. The observed influence can mean that in the case of the Cu-Mn codoping the both nearest Ca4 and Ca5 positions are occupied.

4. Conclusion

From the presented experiments one can make the following conclusions.

1. The radiation induced EPR spectra for the nominally pure HAp and TCP reveal the presence of stable nitrogen containing or hydrogen radicals and depend on the CaP synthesis route. This feature could be exploited for the purity check and determination of the synthesis route/ post synthesis treatment of the "not-well" characterized CaP samples.
2. It is found that the spin Hamiltonian parameters (hyperfine splitting) for the nitrogen containing radicals in TCP differ from those known for HAp that could be connected with the more complicated structure of TCP and presence of different types of stable paramagnetic nitrogen species.
3. Analysis of the EPR spectra of the iron containing CaP allows to determine the presence of iron in Fe^{3+} state even at very low (0.01 wt %) iron concentrations.
4. The observed narrowing of the central EPR line and increase of its amplitude with the concentration of Mn^{2+} in the range from 0.05 up to 5 wt. % could be exploited for the quantitative determination of manganese in CaP.
5. It is shown that the values of the components of g and A for Cu^{2+} ions in TCP are influenced by the presence of the Mn^{2+}. It gives a way to study cation codoping by EPR.

Unfortunately, EPR is still not regarded as a necessary tool for the investigation of CaP materials. We hope that our paper would encourage the specialists in different scientific and industrial branches to use EPR in their studies and routine analyses.

Acknowledgments

The work is supported by the Program of the competitive growth of Kazan Federal University among the world scientific centers. E.K and V.P. acknowledge partial support from Lomonosov Moscow State University Program of Development and Russian Foundation for Basic Research under Grants #15–03–09387, 15–08–99597, 15–29–04871–ofi–m.

References

1. Barinov S. *Russ. Chem. Rev*. **79**, 13 (2010)
2. Uskovic V., Vu V. *Materials* **9**, 434 (2016)
3. Barinov S., Komlev V. *Calcium Phosphate Based Bioceramics for Bone Tissue Engineering*, Trans Tech. Publ: Zuerich (2010), 204 p.
4. Zilm M.E., Chen L., Sharma V., McDannald A., Jain M., Ramprasad R., Wei M. *Phys. Chem. Chem. Phys.* **18**, 16457 (2016)

5. Safronova T., Mukhin E., Putlyaev V., Knotko A., Evdokimov P., Shatalova T., Karpushkin E. *Ceramics International* **43**, 1310 (2017)
6. Vlasova M., Fedotov A., Mendoza Torrez I., Kakazey M., Komlev V., Marquez Aguilar P.. *Ceramics International* **43**, 6221 (2017)
7. Pogosova M., Eliseev A., Kazin P., Azarmi F. *Dyes and Pigments* **141**, 209 (2017)
8. Kaur K., Singh K., Anand V., Islam N., Bhatia G., Kalia N., Singh J. *Ceramics International* **43**, 10097 (2017)
9. Kim B., Nevitt T., Thiele D. *Nat. Chem. Biol*. **4**, 176 (2008)
10. Madsen E., Gitlin J. *Curr. Opin. Gastroenterol*. **23**, 187 (2007)
11. Jonas J., Burns J., Abel E., Cresswell M., Strain J., Paterson C. *Ann. Nutr. Metab.* **37**, 245 (1993)
12. Strause L., Saltman P., Smith K., Bracker M., Andon M. *J Nutr.* **124**, 1060 (1994)
13. Eaton-Evans J., Mcllrath E., Jackson W., McCartney H., Strain J. *J Trace Elem. Exp. Med*. **9**, 87 (1996)
14. Palacios C. *Crit. Rev. Food Sci. Nutr.* **46**, 621 (2006)
15. Bose S., Fielding G., Tarafder S., Bandyopadhyay A. *Trends Biotechnol*. **31**, 594 (2013)
16. Sopyan I., Ramesh S., Nawawi N., Tampieri A., Sprio S. *Ceramics International* **37**, 3703 (2011)
17. Chelyshev Y., Gafurov M., Ignatyev I., Zanochkin A., Mamin G., Sorokin B., Sorokina A., Lyapkalo N., Gizatullina N., Mukhamedshina Y., Orlinskii S.. *BioMed Research Intern.* **2016**, 3706280 (2016)
18. Dong L., Zhu Z., Qiu Y., Zhao J. *Front. Environ. Sci. Eng.* **10**, 28 (2016)
19. Chlala D., Giraudon J., Nuns N., Lancelot C., Vannier R., Labaki M., Lamonier *J. Appl. Catal. B* **184**, 87 (2016)
20. Yang L., Perez-Amodio S., Barrère-de Groot F., Everts V., van Blitterswijk C., Habibovic P. *Biomaterials* **31**, 2976 (2010)
21. Tkachenko M., Kamzin A. *Phys. Solid State* **58**, 763 (2016)
22. Singh R., Srivastava M., Prasad N., Kannan S. *J Alloys Compd*. **725**, 393 (2017)
23. Moreira M., Da Silva Aragão V., De Almeida Soares G., Dos Santos E. *Key Eng Mater* **493-494**, 20 (2012)
24. Kumar G., Thamizhavel A., Yokogawa Y., Kalkura S., Girija E. *Mater. Chem. Phys.* **134**, 1127 (2012)
25. Chlala D., Giraudon J., Nuns N., Lancelot C., Vannier R., Labaki M., Lamonier *J. Appl. Catal. B* **184**, 87 (2016)
26. Gafurov M., Biktagirov T., Mamin G., Klimashina E., Putlayev V., Kuznetsova L., Orlinskii S. *Phys. Chem. Chem. Phys.* **17**, 20331 (2015)
27. Gafurov M., Biktagirov T., Mamin G., Shurtakova D., Klimashina E., Putlyaev V., Orlinskii S. *Phys. Solid State* **58**, 469 (2016)
28. Biktagirov T., Gafurov M., Mamin G., Klimashina E., Putlayev V., Orlinskii S. *J. Phys. Chem. A* **118**, 1519 (2014)
29. Fadeeva I., Gafurov M., Kiiaeva I., Orlinskii S., Kuznetsova L., Filippov Y., Fomin A., Davydova G., Selezneva I., Barinov S. *BioNanoScience* **7**, 434 (2017)
30. Gafurov M., Biktagirov T., Mamin G., Orlinskii S. *Appl. Magn. Reson.* **45**, 1189 (2014)
31. Gafurov M., Biktagirov T., Yavkin B., Mamin G., Filippov Y., Klimashina E., Putlyaev V., Orlinskii S. *JETP Lett.* **99**, 196 (2014)
32. Matković I., Maltar-Strmečki N., Babić-Ivančić V., Sikirić M., Noethig-Laslo V. *Radiat. Phys. Chem.* **81**, 1621 (2012)

33. Stoll S., Schweiger A. *J. Magn. Reson.* **178**, 42 (2006)
34. Klyava Ya.G. *EPR Spectroscopy of Disordered Solids*, Zinatne: Riga (1988), 320 p. (*in Russian*)
35. Mayer I., Diab H., Reinen D., Albrecht C. *J. Mater. Sci.* **28**, 2428 (1993)
36. Mayer I., Jacobsohn O., Niazov T., Werckmann J., Iliescu M., Richard-Plouet M., Burghaus O., Reinen D. *Eur. J. Inorg. Chem.* **7**, 1445 (2003)
37. Pan Y., Chen N., Weil J., Nilges M. *Amer. Miner.* **87**, 1333 (2002)
38. Aminov L., Gafurov M., Korableva S., Kurkin I., Rodionov A. *Phys. Solid State* **59**, 564 (2017)
39. Gafurov M., Yavkn B., Biktagirov T., Mamin G., Orlinskii S., Izotov V., Salakhov M., Klimashina E., Putlayev V., Abdul'yanov V., Ignatjev I., Khairullin R., Zamochkin A., Chelyshev Yu. *Magn. Reson. Solids* **15**, 13102 (2013)
40. Galukhin A., Khelkhal M., Gerasimov A., Biktagirov T., Gafurov M., Rodionov A., Orlinskii S. *Energy Fuels* **30**, 7731 (2016)
41. Pankratov D., Dolzhenko V., Ovchenkov E., Anuchina M., Severin A. *Inorganic Materials* **53**, 89 (2017)
42. Jiang M., Terra J., Rossi A., Morales M., Saitovitch E., Ellis D. *Phys. Rev. B* **66**, 224107 (2002)
43. Sutter B., Wasowicz T., Howard T., Hossner L., Ming D. *Soil Sci. Soc. Am. J.* **66**, 1359 (2002)
44. Yavkin B., Mamin G., Orlinskii S., Gafurov M., Salakhov M., Biktagirov T., Klimashina E., Putlyaev V., Tretyakov Yu., Silkin N. *Phys Chem Chem Phys* **14**, 2246 (2012)
45. Gracheva I., Gafurov M., Mamin G., Biktagirov T., Rodionov A., Galukhin A., Orlinskii S. *Magn Reson Solids* **18**, 16102 (2016)